J. Mech. Phys. Solids 170 (2023) 105125

Contents lists available at ScienceDirect

Journal of the Mechanics and Physics of Solids

journal homepage: www.elsevier.com/locate/jmps

Enhancing the fracture resistance of hydrogels by regulating the energy release rate via bilayer designs: Theory and experiments

Yijie Cai, Jie Ma, Zihang Shen, Xianmin Shao, Zheng Jia *, Shaoxing Qu

State Key Laboratory of Fluid Power and Mechatronic Systems, Key Laboratory of Soft Machines and Smart Devices of Zhejiang Province, Center for X-Mechanics, Department of Engineering Mechanics, Zhejiang University, Hangzhou 310027, China

ARTICLE INFO

Keywords:
Hydrogels
Fracture resistance
Fracture toughness
Energy release rate
Bilayer

ABSTRACT

Hydrogels are becoming increasingly attractive for various practical applications owing to significant improvements in their fracture resistance over the past two decades. Notably, almost all existing methods for enhancing the fracture resistance of hydrogels aim to increase the fracture toughness Γ through multiscale material design. However, engineering the toughness of hydrogels at the material level often requires material-specific, complicated, or expensive synthesis processes. According to the fracture condition $G = \Gamma$, reducing the energy release rate G under given mechanical loads is an alternative way to enhance the fracture resistance. Little efforts, however, have been made to use this approach to enhance the fracture resistance of soft materials such as hydrogels so far, largely due to their highly nonlinear and deformable behavior. This paper formulates a theory for studying the fracture of monolayer and bilayer hydrogel thin films and proposes a structure-based strategy for enhancing the fracture resistance of hydrogels by constructing hydrogel films adhered to underlying stretchable substrates. Through both theoretical analysis and experimental validations, we demonstrate that the strategy exhibits several unique advantages: even a thin and compliant substrate can enhance the fracture resistance of hydrogel films by several folds, and make the fracture resistance of hydrogel films independent of the crack length and the hydrogel size – which dramatically affects the fracture behavior of monolayer hydrogels. The underlying mechanism lies in that the stretchable substrates can effectively constrain the crack opening displacements and reduce the energy release rate G for crack propagation in the hydrogel film. Moreover, the influence of experimentally-observed interfacial delamination on the fracture resistance of substrate-supported hydrogels is also investigated. The present work unveils a first-of-its-kind "structural-toughening" strategy for improving the fracture resistance of hydrogels by structurally regulating the energy release rate.

1. Introduction

Hydrogels are soft materials composed of water-infiltrated polymer networks and possess similar chemical, mechanical, and electrical properties to those of biological tissues, thus holding great promise in biomedical applications such as wound dressing (Wathoni et al., 2016), tissue repair (Qazi and Burdick, 2021) and cell stimulators (Han et al., 2017). Moreover, non-medical applications of synthetic hydrogels have also received extensive attention over the past two decades. The discovery of a series of hydrogels

* Corresponding author.
E-mail address: zheng.jia@zju.edu.cn (Z. Jia).

https://doi.org/10.1016/j.jmps.2022.105125
Received 21 August 2022; Received in revised form 15 October 2022; Accepted 27 October 2022
Available online 29 October 2022

as stretchable, transparent ionic conductors has led to the emergence of a wide range of applications, including ionic loudspeakers (Keplinger et al., 2013), artificial muscles (Haghiashtiani et al., 2018; Li et al., 2017b), artificial skins (Sarwar et al., 2017), ionotronic luminescent devices (Larson et al., 2016), soft robots (Lee et al., 2020) and all-solid-state supercapacitors (Li et al., 2021). The upsurge in the application of synthetic hydrogels in mechanically-demanding environments has stimulated the latest research on the fracture of hydrogels (Cheng et al., 2019, 2020; Yiming et al., 2020). Notably, most hydrogels consisting of sparse polymer networks infiltrated by a large amount of water are brittle, with fracture energies on the order of $10-100\mathrm{J/m^2}$ (Sun et al., 2012). The need for improving the mechanical durability of hydrogels to meet the stringent requirement of soft ionotronics and soft machines has induced an impetus for the development of methods to enhance the fracture resistance of hydrogels.

The fracture resistance of hydrogels can be quantitatively defined by the critical stretch at which a flaw or pre-crack in the hydrogel starts propagating. It is well known that the onset of crack propagation is governed by the critical condition that $G=\Gamma$, where G is the energy release rate and Γ the fracture toughness of hydrogels. Thus far, almost all existing methods for enhancing fracture resistance of hydrogels aim to increase the fracture toughness Γ by multiscale material design. One prominent example is the development of double-network hydrogels consisting of two topologically interpenetrating polymer networks (Chen et al., 2015; Gong et al., 2003; Hagiwara et al., 2010; Liu et al., 2015; Nonoyama and Gong, 2015; Wang et al., 2020; Yin et al., 2020; Zhao, 2012), where the shorter-chain network ruptures to dissipate mechanical energy during deformation and the longer-chain network maintains the elasticity of the hydrogel, thereby imparting high fracture toughness Γ to the hydrogels. In addition, other toughening strategies based on hybrid physical/chemical cross-linkers (Hui and Long, 2012; Kong et al., 2003; Zhao et al., 2010), large crosslinkers with high functionality (Haraguchi and Takehisa, 2002; Seitz et al., 2009; Wang and Gao, 2016; Wang et al., 2010) and meso-/macro-scale fiber/filler reinforcements (Agrawal et al., 2013; Jang et al., 2013; Liao et al., 2013; Moutos et al., 2007) have been proposed to enhance the fracture resistance of hydrogels. Nevertheless, engineering the toughness for hydrogels at the material level often requires material-specific, complicated, or expensive synthesis processes, which are hardly applicable to other materials. Furthermore, for a given hydrogel material whose mechanical properties cannot be redesigned, how to effectively improve the fracture resistance of the given hydrogel remains a challenge.

According to the critical fracture condition that $G=\Gamma$, when the material is given (i.e., the fracture toughness Γ is fixed), reducing the energy release rate G under a given load or deformation is an alternative approach to improve the fracture resistance of the material. In the area of microelectronics and flexible electronics, metal oxide films such as indium tin oxide are widely employed as conductors and electrodes, but they often suffer from fractures under mechanical loadings due to their brittle nature. It has been a common practice in microelectronics to enhance the fracture resistance of the brittle layers by regulating the energy release rate G through structural design. For instance, to meet the stringent requirements of flexible electronics, one commonly used strategy to increase the stretchability of metal oxide films is to attach the films to stretchable polymeric substrates, which can effectively constrain the crack opening displacement when the films fracture, thereby reducing the driving force for crack propagation, achieving the goal of enhancing the fracture resistance of brittle metal oxide films (Cordero et al., 2007; Jia et al., 2011). Thus far, this structure-based approach to enhancing the stretchability of given materials has proven to be successful for hard-material systems, but has not yet been utilized in the field of soft materials, largely due to their highly deformable and nonlinear behavior. To this end, utilizing stretchable substrates to improve the fracture resistance of given hydrogels is of practical significance and warrants further investigation.

Through integrated theoretical analysis and experimental validations, this paper reports a first-of-its-kind structure-based strategy via constructing hydrogel film-substrate bilayers for structurally regulating the energy release rate and enhancing the fracture resistance of hydrogels. The approach has not yet been exploited for soft materials before. Under a given mechanical load, the bilayer design can structurally constrain the crack opening displacement in the hydrogel film and thus regulate the energy release rate for crack propagation, thereby boosting the fracture resistance of hydrogel films. The rest of the paper is organized as follows. Section 2 reports the theoretical analysis of the fracture resistance of hydrogel films adhered to stretchable substrates and monolayer hydrogel films, demonstrating three unique advantages of substrate-supported hydrogel films, which are absent from monolayer hydrogels. Section 3 presents experimental results on fracture tests of monolayer and bilayer hydrogel films, aiming to validate the theoretical predictions and demonstrate the effectiveness of the structure-based strategy. The influence of experimentally observed interfacial delamination on the effectiveness of the fracture-resistance-enhancing approach is also discussed. Conclusions and remarks are given in Section 4.

2. Theoretical analysis

In this section, we demonstrate the effectiveness of the structure-based strategy for enhancing fracture resistance via integrated dimensional considerations and computational modeling. By comparing the calculated fracture resistance of monolayer hydrogel films and hydrogel films attached to stretchable substrates, we show that even a thin and compliant substrate can enhance the fracture resistance of hydrogel by several folds. It is also revealed that the fracture resistance of substrate-supported hydrogel thin films is independent of the crack length and hydrogel size, a highly desirable feature absent for freestanding hydrogel films.

2.1. Description of the strategy for enhancing fracture resistance of hydrogels

As mentioned above, the fracture resistance of hydrogels can be defined by their stretchability, i.e., the critical stretch at which the flaw or pre-crack starts propagating. To illustrate the main idea, we consider a pre-notched monolayer hydrogel thin sheet subject to uniaxial stretching. As illustrated in Fig. 1a I, the pre-crack opens continuously – with uniform crack opening displacement across the sheet thickness – as the applied stretch increases, and eventually turns into a running crack at a moderate stretch level λ_{cr}^{m}. To enhance the fracture resistance of the given hydrogel sheet, we propose to adhere it to stretchable soft substrates. As shown in Fig. 1a II, the

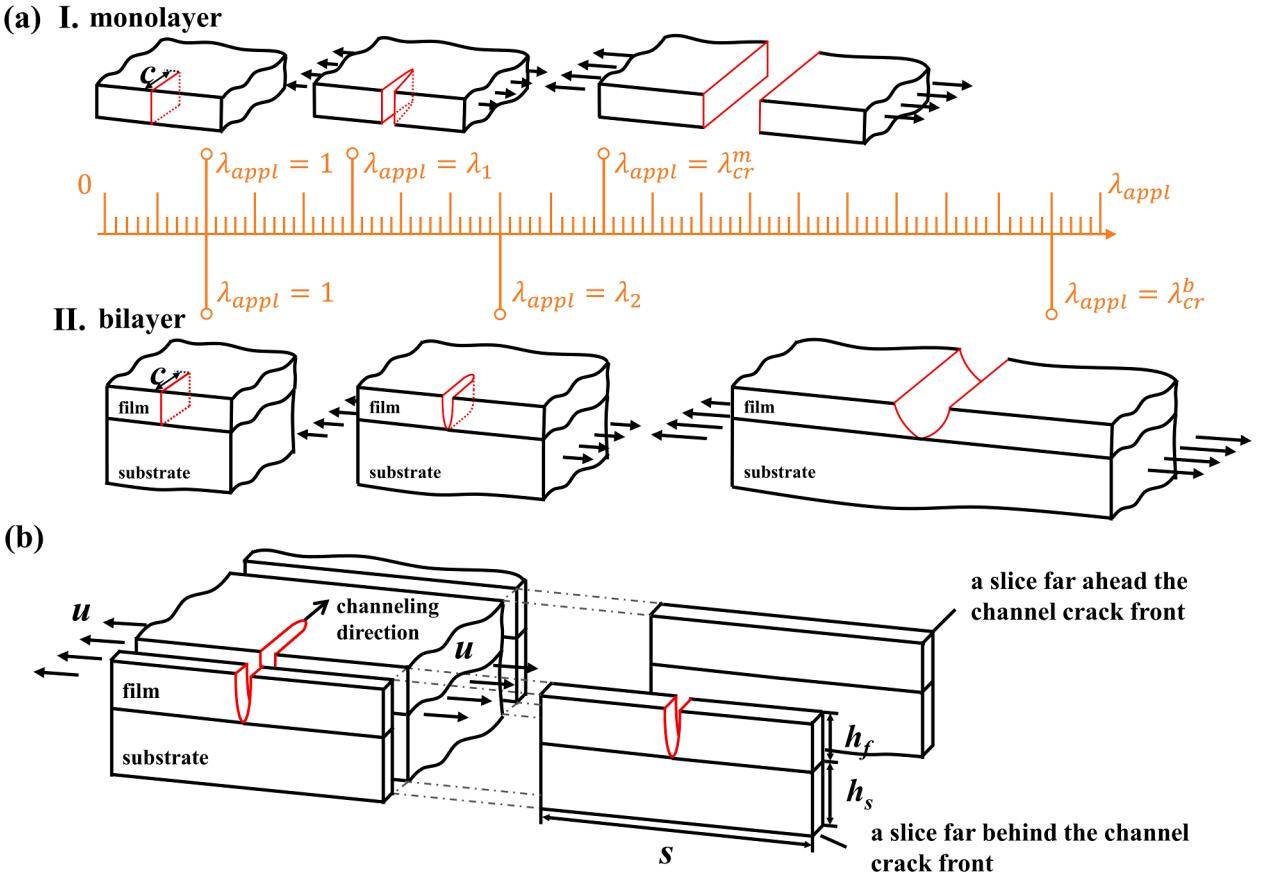

Fig. 1. Schematics illustrating the structure-based strategy for enhancing fracture resistance of hydrogels by regulating energy relate rate. (a) I. A monolayer hydrogel thin sheet with a pre-crack of length c subject to uniaxial stretch. The pre-crack starts to propagate at a moderate stretch level λ_{cr}^m. II. A bilayer hydrogel structure formed by adhering the thin hydrogel film with a pre-crack of length c to a stretchable soft substrate. The pre-crack does not propagate until the applied stretch reaches λ_{cr}^b ($\lambda_{cr}^b > \lambda_{cr}^m$). The underlying substrate turns a uniform crack into a channel crack, thereby reducing the energy release rate and enhancing the fracture resistance of the hydrogel film. (b) The computational model for calculating the energy release rate of steady-state channel crack in a bilayer hydrogel structure. The elastic energy released by the channel crack advancing a unit distance equals to the elastic energy stored in a slice of material of unit thickness far ahead of the crack front minus the elastic energy stored in a slice of material of unit thickness far behind the crack front.

underlying stretchable substrate can mechanically constrain the crack opening displacement by turning the uniformly opened crack into a channel crack. According to fracture mechanics analysis (Cordero et al., 2007), the amount of energy released due to crack propagation is related to the crack opening displacement – the larger the crack opening displacement, the higher the energy release rate. Due to the mechanical constraint of the substrate, the energy release rate of such channel cracks is lower than that of uniformly-opened cracks in monolayer hydrogel sheets. For this reason, the underlying stretchable substrate can carry the pre-notched hydrogel film to a higher critical stretch λ_{cr}^{b} ($\lambda_{cr}^{b} > \lambda_{cr}^{m}$). Thus, the substrate-supported hydrogel thin film should exhibit enhanced fracture resistance relative to the monolayer hydrogel film. In Sections 2.2 and 2.3, we will quantitatively demonstrate the effectiveness of the fracture-resistance enhancement strategy by integrating dimensional analysis and finite element calculations.

2.2. Fracture resistance of substrate-supported hydrogel films

To quantitatively reveal the effectiveness of this structure-based strategy for enhancing the fracture resistance of hydrogels, we analyze the driving force (i.e., the energy release rate) for fracture propagation in a film-substrate bilayer hydrogel structure shown in Fig. 1a II. All materials in the structure are taken to be hyperelastic and incompressible. The two layers are assumed to be well bonded. The entire structure is subject to a stretch λ_{appl} parallel to the layers. Let U be the elastic energy released by the steady-state channel crack advancing a unit distance. As illustrated in Fig. 1b, the released elastic energy U can be calculated as follows: the elastic energy stored in a slice of material of unit thickness far ahead of the crack front minus the elastic energy stored in a slice of material of unit thickness far behind the crack front (Hutchinson and Suo, 1991). The elastic energies of the two slices far ahead and far behind the channel crack front can be conveniently obtained by numerically solving two plane-strain boundary-value problems. Moreover, dimensional considerations suggest that this reduction in elastic energy takes the form

$$U = f\left(\frac{h_s}{h_f}, \frac{\mu_s}{\mu_f}, \lambda_{appl}\right)\mu_f h_f^2. \tag{1}$$

Herein, h_f and h_s are the thickness of the hydrogel film and substrate, respectively. μ_f and μ_s are the shear modulus of the hydrogel film and substrate, respectively. λ_{appl} denotes the applied stretch. The dimensionless function f depends on three dimensionless numbers including the thickness ratio h_s/h_f, the shear modulus ratio μ_s/μ_f, and the applied stretch λ_{appl}. Then the energy release rate associated with the channel crack advancing in the direction perpendicular to the applied stretch can be written as:

$$G^b = U/h_f = f\left(\frac{h_s}{h_f}, \frac{\mu_s}{\mu_f}, \lambda_{appl}\right)\mu_f h_f, \tag{2}$$

where the superscript b refers to bilayer hydrogel structures. The normalized energy release rate for channel cracking in substrate-supported hydrogel film can be defined as:

$$\frac{G^b}{\mu_f h_f} = f\left(\frac{h_s}{h_f}, \frac{\mu_s}{\mu_f}, \lambda_{appl}\right), \tag{3}$$

such that the normalized energy release rate $G^b/\mu_f h_f$ is a function of the three dimensionless numbers, including h_s/h_f, μ_s/μ_f, and λ_{appl}.

To evaluate the normalized energy release rate $G^b/\mu_f h_f$ for any given combination of h_s/h_f, μ_s/μ_f, and λ_{appl}, as shown in Fig. 1b, we model a slice of material of unit thickness far ahead of the channel crack front and a slice of material of unit thickness far behind the crack front. The simulations are conducted using the commercial finite element package ABAQUS. The calculated elastic energy difference between the two slices gives the elastic energy reduction U in Eq. (1). Then, the normalized energy release rate $G^b/\mu_f h_f$ is given by $U/\mu_f h_f^2$. The neo-Hookean model is adopted in the simulations for the hydrogel films and substrates. The Poisson's ratio is set to 0.49 for both the film and substrate to model the nearly incompressible behavior of hydrogels. The length of the slices s is set to be $s = 100h_f$. The slices are meshed with the CPE4 element (i.e., the four-node bilinear plane strain quadrilateral element). For the slice far behind the crack front, the region in the proximity of the channel crack root is densely meshed. Regarding boundary conditions, the displacement u, which is parallel to the hydrogel layers, is exerted on the lateral sides of the slices, yielding an applied stretch of $\lambda_{appl} = u/50h_f + 1$. In the simulations, as suggested by Eq. (1), we vary the thickness ratio h_s/h_f and the shear modulus ratio μ_s/μ_f, respectively, to study their effect on the energy release rate for channel cracking in substrate-supported hydrogel films.

Fig. 2a plots the calculated normalized energy release rate $G^b/\mu_f h_f$ as a function of the applied stretch λ_{appl} for various thickness ratios h_s/h_f, with shear modulus ratio fixed at $\mu_s/\mu_f = 0.1$. In contrast, in plotting Fig. 2b, we set the thickness ratio $h_s/h_f = 5$ but vary the shear modulus ratio μ_s/μ_f. As evident in Fig. 2a and b, the normalized energy release rate rises with increasing applied stretches and decreases when the thickness or the modulus of the substrate increases. The trends can be understood as follows: the crack opening displacement in the top hydrogel film is constrained by the bottom hydrogel substrate; a stiff and thick substrate can more effectively restrain the opening of cracks. Therefore, the thicker and stiffer the substrate, the lower the driving force $G^b/\mu_f h_f$ for channel cracking in substrate-supported hydrogel film.

A crack will propagate in the hydrogel film if the elastic energy reduction U exceeds the fracture energy Γ_f times the film thickness h_f. Hence, the critical condition for the steady-state crack propagation can be defined as:

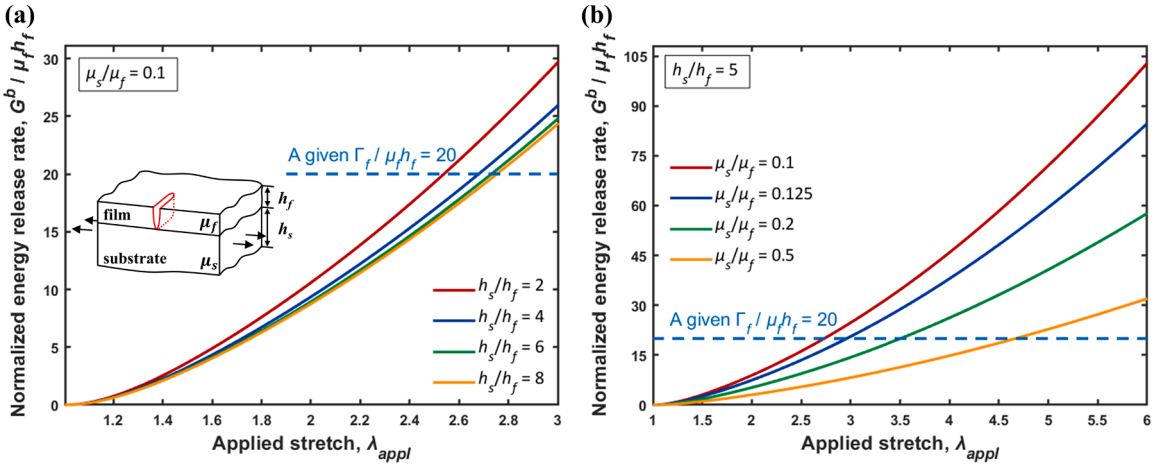

Fig. 2. The normalized energy release rate for steady-state channel cracking in substrate-supported hydrogel film. (a) $G^b/\mu_f h_f$ plotted as a function of the applied stretch λ_{appl} for various normalized substrate thickness h_s/h_f. The shear modulus ratio μ_s/μ_f is fixed to 0.1. Inset: schematics of the substrate-supported hydrogel film. (b) $G^b/\mu_f h_f$ as a function of the applied stretch λ_{appl} for various normalized substrate shear modulus μ_s/μ_f. The fixed thickness ratio $h_s/h_f = 5$ is used.

$$U = \Gamma_f h_f. \tag{4}$$

Combining Eqs. (2) and (4) yields that the critical condition for channel cracking can be recast in terms of the energy release rate G^b,

$$G^b = \Gamma_f. \tag{5}$$

By substituting Eq. (5) into Eq. (3), we can rewrite the critical condition for steady-state channel cracking in a dimensionless form that

$$f\left(\frac{h_s}{h_f}, \frac{\mu_s}{\mu_f}, \lambda_{cr}^b\right) = \frac{\Gamma_f}{\mu_f h_f}. \tag{6}$$

The geometric significance of Eq. (6) is illustrated in Fig. 2: once the normalized fracture toughness $\Gamma_f/\mu_f h_f$ (represented by the horizontal dashed lines in Fig. 2) of the hydrogel film is given, one can determine the critical stretch λ_{cr}^b – at which the channel crack in the hydrogel film starts propagating steadily – by finding the intersection of the dashed line and the calculated energy release rate curve in Fig. 2. In this work, without loss of generality, we take $\Gamma_f/\mu_f h_f = 20$, which corresponds to $\Gamma_f = 100\text{J/m}^2$, $\mu_f = 5\text{kPa}$, and $h_f = 1\text{mm}$. These values are typical for PAAm hydrogels or PAA hydrogels, which are widely referred to as stretchable soft materials (Lake and Thomas, 1967; Wang et al., 2019; Yang et al., 2019; Yao et al., 2021).

Fig. 3a and b summarize critical stretches λ_{cr}^b for channel cracking in substrate-supported hydrogel film as a function of the normalized substrate thickness h_s/h_f and normalized substrate shear modulus μ_s/μ_f, respectively. In Fig. 3a, it can be observed that the critical stretch rises as the substrate thickness increases, and gradually approaches a plateau when the substrate becomes sufficiently thick. This trend can be explained as follows: for a thick substrate, the bottom portion of the substrate is far from the hydrogel film and thus has a negligible impact on the crack formation in the film. Meanwhile, Fig. 3b shows that increased substrate shear modulus enhances the critical stretch λ_{cr}^b for channel cracking. According to the results shown in Fig. 3, improving the substrate modulus is proved to be a more effective approach to enhancing the fracture resistance of hydrogel film than adjusting the substrate thickness. For example, when the normalized substrate thickness is fixed to be $h_s/h_f = 2$ that represents a relatively thin substrate, the critical stretch λ_{cr}^b increases by a factor of ~1.75 – from 2.058 to 3.6 – as μ_s/μ_f increases from 0.05 to 0.25 (Fig. 3b). In contrast, by changing h_s/h_f from 1 to 8 (Fig. 3a), the increments of λ_{cr}^b are all less than 20% – from 1.947 to 2.228 for $\mu_s/\mu_f = 0.005$, 2.351 to 2.759 for $\mu_s/\mu_f = 0.1$, and 3.055 to 3.529 for $\mu_s/\mu_f = 0.2$, respectively.

2.3. Comparison of fracture resistance between substrate-supported hydrogel films and monolayer hydrogel films

In Section 2.2, we have analyzed the fracture resistance of substrate-supported hydrogel films, which is defined by the critical stretch that triggers steady-state crack propagation. In this section, we will investigate the fracture resistance of monolayer hydrogel sheets. The critical stretches for crack propagation will be compared between monolayer hydrogels and substrate-supported hydrogels, aiming to quantitatively demonstrate the effectiveness of the bilayer structural design strategy in enhancing the fracture resistance of hydrogels.

To study the fracture resistance of monolayer hydrogel sheets, we consider a pre-notched thin hydrogel film subject to uniaxial elongation u (Fig. 4a). The deformation of the hyperelastic hydrogel film can be obtained by numerically solving a plane-stress

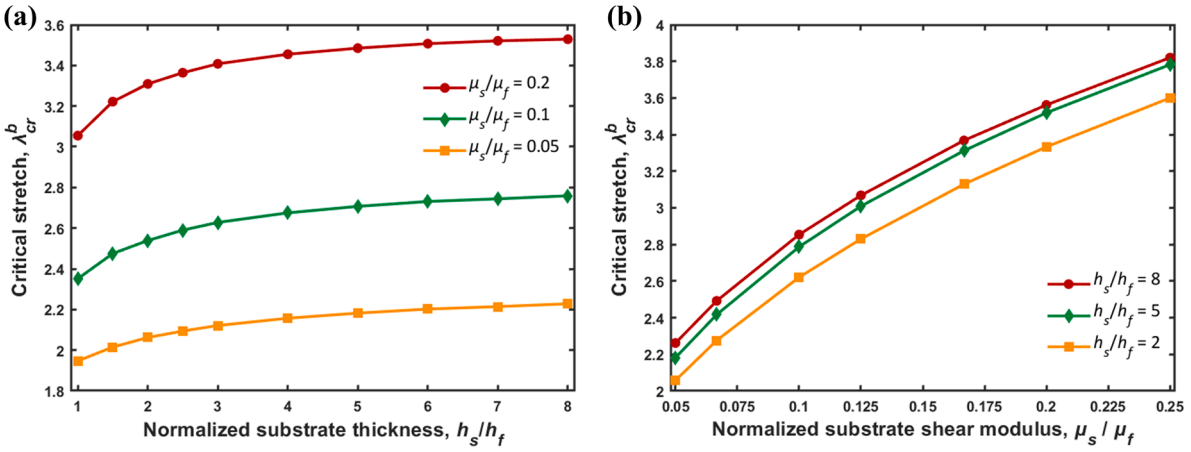

Fig. 3. The critical stretch λ_{cr}^b for steady-state channel cracking in substrate-supported hydrogel film. Given the normalized fracture toughness of the hydrogel film $\Gamma_f/\mu_f h_f$, the critical stretch λ_{cr}^b at which the channel crack in the hydrogel film propagates steadily can be plotted as a function of (a) the normalized substrate thickness h_s/h_f and (b) the normalized substrate shear modulus μ_s/μ_f.

boundary-value problem. Assuming that the length s of the hydrogel sheet is much larger than other dimensions, the only length scales that remain in the boundary-value problem are the crack length c and the film width w. In this respect, dimensional considerations dictate that the energy release rate G^m associated with the advancement of the pre-crack takes the form that

$$G^m = g\left(\frac{c}{w}, \lambda_{appl}\right)\mu_f c. \tag{7}$$

Herein, the superscript m refers to monolayer hydrogel films. μ_f is the shear modulus of the hydrogel film, and the dimensionless function g depends on the two dimensionless numbers: the ratio of crack length to the sheet width c/w, and the applied stretch λ_{appl} defined as $\lambda_{appl} = 2u/s + 1$. Furthermore, we can write the normalized energy release rate as follows:

$$\frac{G^m}{\mu_f c} = g\left(\frac{c}{w}, \lambda_{appl}\right). \tag{8}$$

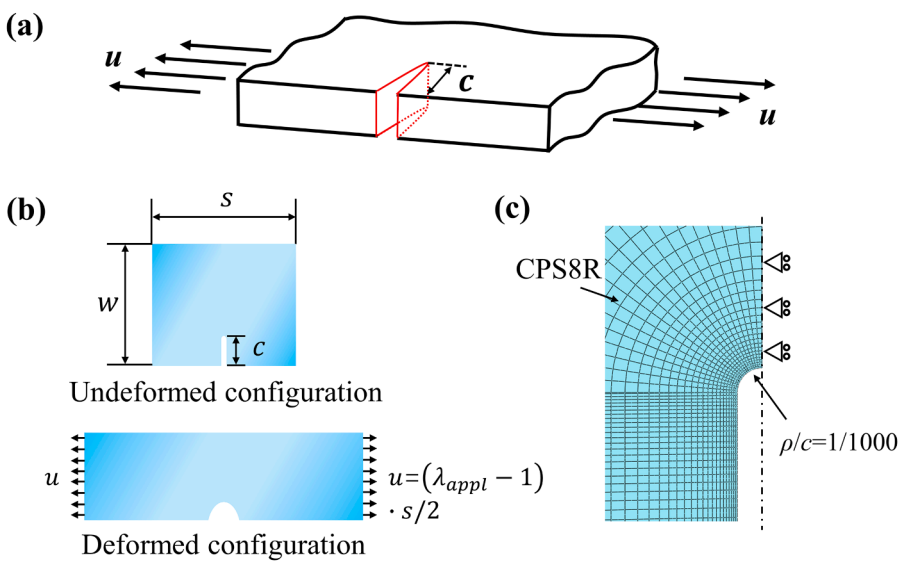

Fig. 4. Computation model for calculating the energy release rate for crack propagation in monolayer hydrogel sheets. (a) Schematics of a hydrogel sheet with a pre-crack of length c. (b) The characteristic dimensions of the pre-notched hydrogel sheet. In the undeformed state, the width and length of the sheet are w and s, respectively. The length of the crack is c. In the deformed state, the hydrogel sheet is pulled to a length of $\lambda_{appl}s$. (c) The blunted crack tip modeled with a finite radius ρ. The hydrogel sheet is densely meshed with CPS8R elements in ABAQUS.

The energy release rate G^m can be directly calculated as the J-integral (Rice, 1968) using the finite element package ABAQUS. Then, values of the dimensionless function $g\left(\frac{c}{w}, \lambda_{appl}\right)$ can be computed according to Eq. (8). In the simulations, we model a pre-notched hydrogel sheet with sample length s, width w, and crack length c, as shown in Fig. 4b. Here, we assume $s = 40w$ to model a long hydrogel sheet, which is stretched by a horizontal displacement u. Neo-Hookean model with nearly incompressible mechanical behavior (Poisson's ratio is set to 0.49) is adopted for the hydrogel. By taking advantage of the symmetry of the geometry, only half of the hydrogel sheet is modeled, with the symmetric boundary condition set along the symmetry plane and the displacement u applied to the lateral side of the model. To avoid singularity at the crack tip in the simulation, we model a blunt crack tip with a small radius $\rho = c/1000$ in the undeformed configuration. The model is meshed with CPS8R elements, with dense meshes in the region near the crack tip (Fig. 4c). In the simulations, we vary the ratio c/w to study the driving force for crack propagation in the monolayer hydrogel sheet. Fig. 5 plots the calculated normalized driving force $G^m/\mu_f c$ for crack propagation as a function of the applied stretch λ_{appl} for various ratios c/w. The trend of the curves indicates that a higher c/w leads to a more significant driving force. That is, for a given hydrogel sheet, longer cracks result in higher energy release rates. Moreover, according to Eq. (8), Fig. 5 also gives the value of the dimensionless function $g\left(\frac{c}{w}, \lambda_{appl}\right)$, which will be used later to determine the critical stretch of monolayer hydrogel films.

The pre-formed crack of length c in monolayer hydrogel sheets starts to propagate when the energy release rate reaches the fracture toughness of the hydrogel film, i.e.,

$$G^m = \Gamma_f, \tag{9}$$

such that the critical stretch λ_{cr}^m for crack propagation can be obtained by numerically solving the following dimensionless equation when the value of c/w is given,

$$\frac{\Gamma_f}{\mu_f c} = g\left(\frac{c}{w}, \lambda_{cr}^m\right). \tag{10}$$

It is worth noting that the value of $\Gamma_f/\mu_f h_f$ is a constant for a given monolayer hydrogel sheet. In contrast, the dimensionless number $\Gamma_f/\mu_f c$ varies with the crack length c and thus is not a characteristic constant for the hydrogel film. For this reason, to determine the critical stretch for any given monolayer hydrogel sheet, Eq. (10) can be rewritten as:

$$\frac{\Gamma_f}{\mu_f h_f} = \left(\frac{w}{h_f}\right) p\left(\frac{c}{w}, \lambda_{cr}^m\right), \tag{11}$$

where the dimensionless function $p\left(\frac{c}{w}, \lambda_{appl}\right) = \left(\frac{c}{w}\right) g\left(\frac{c}{w}, \lambda_{appl}\right)$. As mentioned above, the dimensionless function $g\left(\frac{c}{w}, \lambda_{appl}\right)$ can be calculated using the finite element code ABAQUS and is shown in Fig. 5. Once the normalized fracture toughness $\Gamma_f/\mu_f h_f$ of the hydrogel film is given, critical stretch λ_{cr}^m for the monolayer hydrogel sheet of normalized crack length c/w can be determined using Eq. (11). Here we take $\Gamma_f/\mu_f h_f = 20$, a value typical for PAAm and PAA samples (Lake and Thomas, 1967; Wang et al., 2019; Yang et al., 2019; Yao et al., 2021). Fig. 6 plots critical stretch λ_{cr}^m for monolayer hydrogel sheets as a function of normalized crack length c/w with various width-to-thickness ratios w/h_f. The results will be discussed in detail later.

To facilitate the comparison of fracture resistance between substrate-supported hydrogel films and monolayer hydrogel films, we compare a monolayer hydrogel film of width w, thickness h_f, and crack length c to the same hydrogel film of the same sizes adhered to a

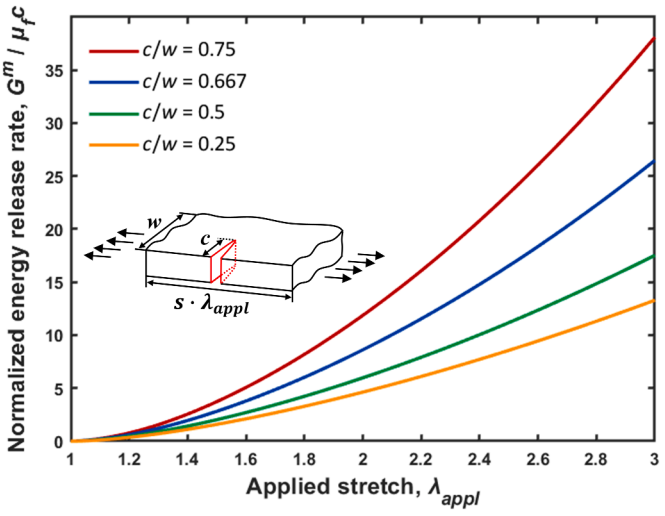

Fig. 5. Normalized energy release rate $G^m/\mu_f c$ for crack propagation in monolayer hydrogel films as a function of the applied stretch λ_{appl} for various relative crack lengths c/w. Inset: schematics of a monolayer hydrogel sheet with a pre-crack of length c.

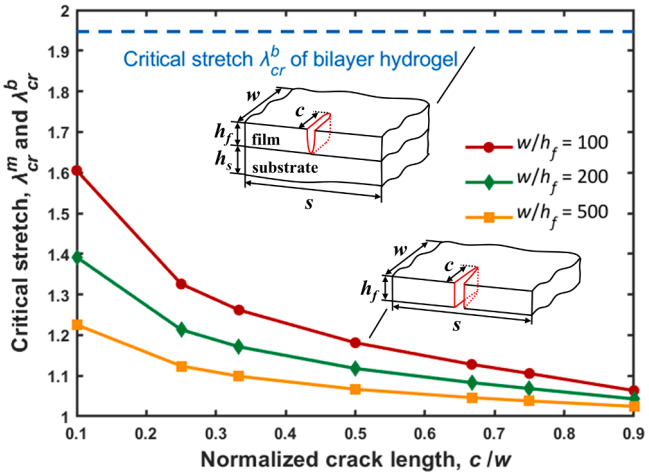

Fig. 6. Comparison of critical stretches between substrate-supported hydrogel films and monolayer hydrogel films. The critical stretches λ_{cr}^{m} of monolayer hydrogel films are a function of the normalized crack length c/w and depend on the hydrogel size w/h_f. In stark contrast, the critical stretch λ_{cr}^{b} of substrate-supported hydrogel films well exceeds that of monolayer hydrogel sheets and, intriguingly, is independent of the normalized crack length c/w and in-plane dimension $w/h_f$of the sheets. Insets: schematics of the monolayer hydrogel sheets and substrate-supported hydrogel films.

stretchable substrate. For the substrate-supported hydrogel film, we consider attaching the hydrogel film with normalized fracture toughness $\Gamma_f/\mu_f h_f = 20$ to thin and compliant substrates characterized by $h_s/h_f = 1$ and $\mu_s/\mu_f = 0.05$. According to the results shown in Fig. 3a, the critical stretch λ_{cr}^{b} for channel crack propagation in the bilayer hydrogel system – which is dictated by Eq. (6) – is ~ 1.95 (dashed line in Fig. 6).

By comparing critical stretches between monolayer hydrogel sheets and substrate-supported hydrogel films (shown in Fig. 6), we find three unique advantages of substrate-supported hydrogel films:

- First, substrate-supported hydrogel films exhibit significantly enhanced fracture resistance (i.e., critical stretch) relative to monolayer hydrogel films. As evident in Fig. 6, the critical stretch of substrate-supported hydrogel films (the dashed line in Fig. 6) is considerably higher than those of monolayer hydrogel sheets (the solid lines), demonstrating that even simply adding a thin and compliant stretchable substrate ($h_s/h_f = 1$ and $\mu_s/\mu_f = 0.05$) can result in a considerable increase in the fracture resistance of hydrogel sheets. Moreover, according to the results shown in Fig. 3, if a stiff substrate is used (e.g., $\mu_s/\mu_f = 0.2$), the critical stretch can almost triple that of the monolayer hydrogel. In other words, the substrate-supported hydrogel film can withstand much higher elongations before rupture than monolayer hydrogel sheets, regardless of the modulus and thickness of the underlying substrate. Hence, adding a stretchable substrate is a simple but rather effective structural design strategy to regulate the energy release rate and enhance the fracture resistance of the hydrogel.
- Second, the fracture resistance of substrate-supported hydrogel films is not influenced by the crack length c/w, apparently different from monolayer hydrogel films. Fig. 6 shows that, for a given hydrogel film with fixed normalized width w/h_f, the critical stretch of monolayer hydrogel – which decreases continuously with increasing normalized crack length c/w – is strongly affected by the size of the pre-crack. In sharp contrast, the critical stretch of the substrate-supported hydrogel film is independent of the normalized crack length c/w. This can be explained by the concept of steady-state crack propagation: a classic study by Hutchinson and Suo (1991) has shown that upon the crack length c reaching a few times the film thickness, the channel crack will progressively reach a steady-state – the shape of the entire crack front remains the same as it advances, and thus the energy released associated with the crack advancing a unit distance becomes irrelevant to the crack length. To this end, distinct from monolayer hydrogel films, fracture resistance of substrate-supported hydrogel films is insensitive to the flaw size, a highly desirable mechanical feature for practical applications of hydrogels. Note here that the above conclusion holds only when the condition for steady-state crack propagation is met: For a thin film ($w >> h_f$), the crack length c should exceed a few times the film thickness h_f and should not be very close to the film width w.
- Third, when the condition for steady-state crack propagation is satisfied, the fracture resistance of substrate-supported hydrogel films is independent of the in-plane dimensions of the hydrogel film, in striking contrast to monolayer hydrogel films. As shown in Fig. 6, in which the hydrogel film thickness h_f is kept the same for all cases studied, with any given normalized crack length c/w, the critical stretches of monolayer hydrogel films decrease with the hydrogel's in-plane dimension w, which is in line with Eq. (7) – the energy release rate for crack propagation in monolayer hydrogel sheets is proportional to the crack length c. In other words, at a given normalized crack length c/w, the larger the hydrogel sheet, the lower the critical stretch, which reduces the mechanical reliability of monolayer hydrogel sheets of large sizes and hinders their practical applications in mechanically demanding environments. Notably, as revealed by the horizontal dashed line in Fig. 6, adhering hydrogel films to stretchable substrates can

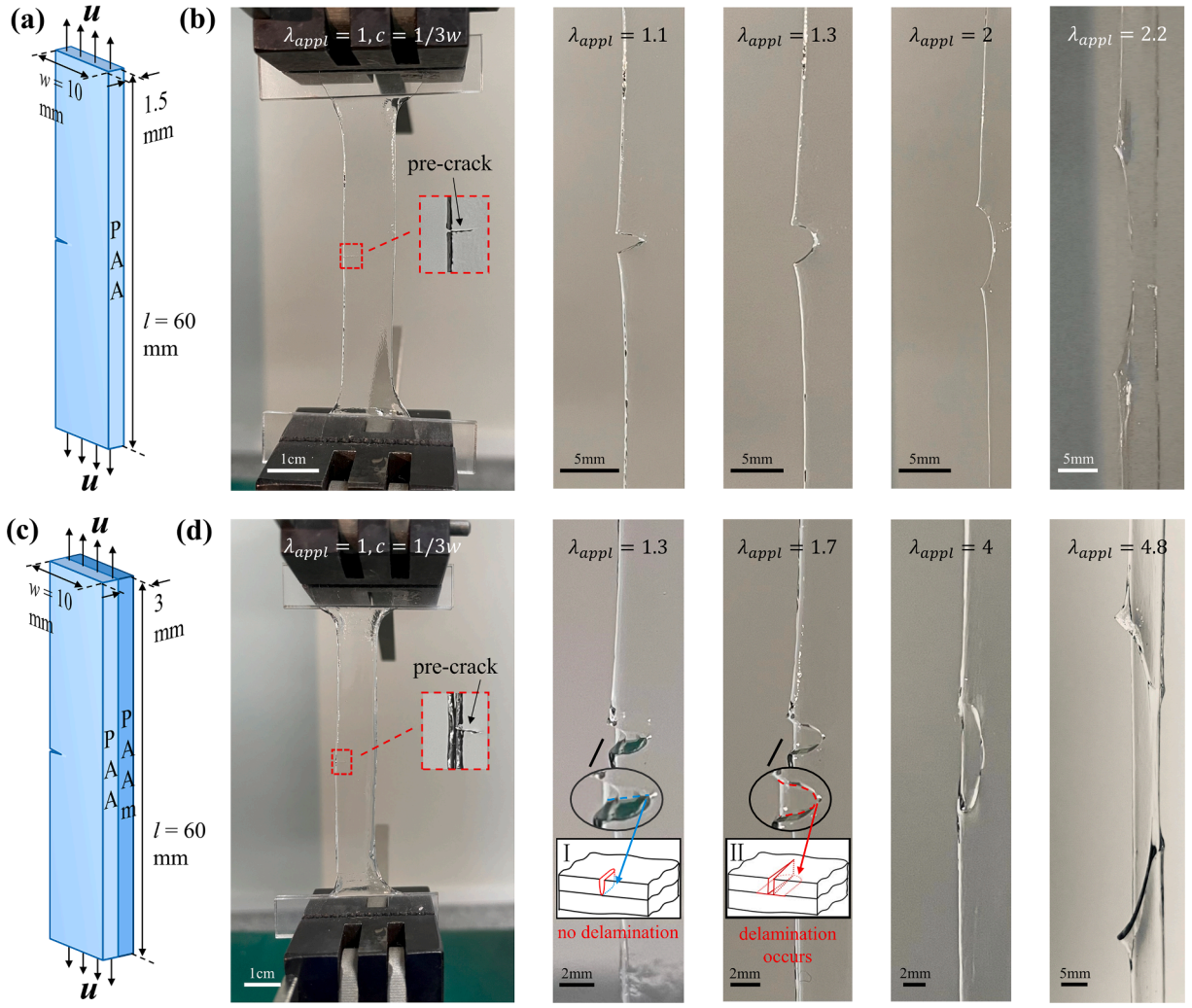

Fig. 7. Results of uniaxial tension tests of monolayer PAA hydrogels and PAAm-supported PAA hydrogels. (a) Schematics of the monolayer PAA sample being tested. The dimensions of the tested sample are 60 mm (gauge length between grips) × 10 mm (width) × 1.5 mm (thickness). The normalized crack length is $c/w = 1/3$. (b) Photos of monolayer PAA hydrogel sheets subject to various stretches. The pre-notched monolayer PAA sheet ruptures at a critical stretch of $\lambda_{cr}^{m} = 2.2$. (c) Schematics of the bilayer hydrogel structure consisting of a PAA film adhered to a PAAm substrate. Both the film and substrate have dimensions of 60 mm × 10 mm × 1.5 mm. A precut with normalized crack length of $c/w = 1/3$ is introduced in the PAA layer. (d) Photo snapshots of PAAm-supported PAA sheets during stretching. The pre-crack in the bilayer structure remains stationary until the stretch reaches $\lambda_{cr}^{b} = 4.8$, showing significantly enhanced fracture resistance. Inset I and II: schematics showing the crack morphology without and with interfacial delamination, respectively.

eliminate the size dependence of the fracture resistance of hydrogel films, thereby boosting their fracture resistance, especially when the hydrogel films are large. The reason is that the energy release rate for channel cracking in substrate-supported hydrogel films is independent of the in-plane dimensions of the gel. Taking advantage of this desirable characteristic of substrate-supported hydrogel films, even if a hydrogel sheet is large in size and thus liable to fracture, we can adopt the bilayer structural design strategies to effectively improve its fracture resistance.

In summary, in this section, we theoretically demonstrate that adhering hydrogel sheets to stretchable substrates can effectively enhance the fracture resistance – the critical stretch at which crack starts propagating – of the hydrogel sheets, by rendering the energy release rate independent of the in-plane dimensions of the hydrogel sheets and the flaw size.

3. Experimental section

We have theoretically shown that adding a stretchable substrate can effectively enhance the fracture resistance of hydrogel sheets. In this section, we will further experimentally validate the theoretical predictions presented in Section 2 by conducting uniaxial tensile

tests on substrate-supported and monolayer hydrogel films, aiming to demonstrate the effectiveness of the proposed fracture-resistance enhancing method based on the bilayer structure design.

3.1. Material selection

To validate the fracture-resistance enhancement method, we need to first design and fabricate the bilayer hydrogel structure consisting of two distinct hydrogel layers – including the hydrogel film and the stretchable hydrogel substrate. To ensure the two layers can adhere well and fast, we choose polyacrylamide (PAAm) hydrogels and poly-(acrylic acid) (PAA) hydrogels to make the bilayer structure based on an established fact in chemistry: the carboxyl groups on PAA and the amide groups on PAAm can form hydrogen bonds (Wang et al., 2019), endowing instant and tough adhesion between PAA and PAAm hydrogels.

3.2. Preparation of hydrogels

The hydrogel monomers are purchased from Macklin, including acrylic acid (AA, A800293) and acrylamide (AAm, A800656). The following chemicals are purchased from Sigma-Aldrich: N, N'-methylenebis (acrylamide) (MBAA, M7279), α-ketoglutaric acid (75890). All chemicals are used directly upon receipt without further purification.

To synthesize the PAA hydrogel, we add 6.255 g AA, 0.0088 g N, N′-methylenebis (acrylamide) (MBAA, 0.14 wt% of AA), and 0.0125 g α-ketoglutaric acid (0.2 wt% of AA) into 30 ml of deionized water sequentially to obtain the precursor solution for PAA hydrogel. The AA, MBAA, and α-ketoglutaric acid are the monomer, cross-linker, and photo-initiator, respectively. We then inject the precursor solution into a mold consisting of two pieces of acrylic plates separated by an acrylic spacer. Note that the mold is treated with commercial glass water repellent before the injection of precursor solution to prevent the PAA hydrogel from adhering to the acrylic mold. After curing under 365 nm UV radiation for 2 h, we obtain a thin rectangular PAA hydrogel sheet with the dimensions of 70 mm (length) × 10 mm (width) × 1.5 mm (thickness).

To synthesize the PAAm hydrogel, we add 6.809 g AAm into 50 ml of deionized water. Then 0.0041 g MBAA (0.06 wt% of AAm) and 0.0136 g α-ketoglutaric acid (0.2 wt% of AAm) are added to the aqueous solution as the cross-linker and the photo-initiator, respectively. The precursor solution is then injected into the mold, which is treated with commercial glass water repellent in advance, and subjected to 365 nm UV radiation (8 W) for 1 h for curing. The mold shapes the synthesized PAAm hydrogel into a rectangular sheet with sizes of 70 mm × 10 mm × 1.5 mm, the same as that of the PAA hydrogel sheet.

To fabricate the bilayer hydrogel structures, i.e., the PAA hydrogel film adhered to the PAAm substrate. As-synthesized PAA hydrogels and PAAm hydrogels are removed from the mold with tweezers and immediately put in clean sample bags separately to avoid contamination. After 20 min, we take out the PAAm and PAA hydrogels from the sample bag, introduce a precut in the PAA hydrogel with a razor blade, and immediately bring the two hydrogel sheets together at ambient conditions without applying any contact pressure. The contact time is set to 30 s before testing. Instant and tough adhesion between the two layers forms fast due to the noncovalent hydrogen bonds formed between the carboxyl groups on PAA and the amide groups on PAAm, as expected.

3.3. Mechanical testing

To compare the fracture resistance of monolayer PAA hydrogels and PAA hydrogels supported by PAAm substrates, we conduct uniaxial tensile tests on both pre-cracked PAA hydrogel sheets (Fig. 7a) and pre-cracked PAA sheets adhered to unnotched PAAm substrates (Fig. 7c). All tensile tests are performed using the mechanical testing machine SAS CMT-6103 with a 50 N load cell. Before testing, each end of the prepared hydrogel samples is sandwiched by two acrylic plates, and then the entire structure is clamped at both ends to the clamping fixtures of the testing machine. The sample length between the two grips of the testing machine is about 60 mm. The hydrogels are stretched in the direction perpendicular to the pre-crack with a loading rate of 30 mm/min, yielding a strain rate of ~0.83% per second.

Fig. 7b and d illustrate the deformation and rupture processes of monolayer and bilayer hydrogel structures under uniaxial tension, respectively. Both structures contain a pre-crack in the PAA layer with a normalized crack length c/w of 1/3. As shown in Fig. 7b, the pre-crack in the monolayer PAA hydrogel sheet gradually opens with increasing applied stretch, becomes blunt at a stretch of $\lambda_{appl} = 2$, and eventually turns into a running crack at $\lambda_{cr}^{m} = 2.2$, fracturing the PAA hydrogel sheet. Fig. 7d demonstrates that, for PAAm-supported PAA hydrogel films, crack opening displacement increases as the applied stretch increases. Notably, at similar stretch levels, the crack opening displacement in the PAAm-supported PAA film is markedly lower than that in the monolayer PAA film, resulting in significantly reduced energy release rate for crack propagation, largely due to the constraint from the underlying PAAm substrate. As a result, the PAAm-supported PAA film can sustain much higher stretches than the monolayer PAA sheet. As evident in Fig. 7d, although the pre-crack becomes highly blunt upon a stretch of $\lambda_{appl} = 4$, it remains stationary until the stretch reaches $\lambda_{cr}^{b} = 4.8$, which roughly doubles that of a monolayer PAA sheet. The results reveal the effectiveness of the structure-based strategy: the PAAm substrate can effectively enhance the fracture resistance of PAA hydrogels.

Moreover, one salient feature of the stretched bilayer PAAm-PAA hydrogel structure is the interfacial delamination near the crack. It can be recognized in Fig. 7d that at the stretch of $\lambda_{appl} = 1.3$ (i.e., the early stage of stretching), the interfacial delamination has not taken place. The root of the channel crack is well bonded to the substrate so that the cross-section of the crack is V-shaped. That is, as illustrated in Inset I of Fig. 7d, the two crack surfaces are connected at the channel root, which is consistent with the computational model described in Fig. 1a II. However, at the stretch of $\lambda_{appl} = 1.7$ and 4, interfacial delamination occurs in the proximity of the crack.

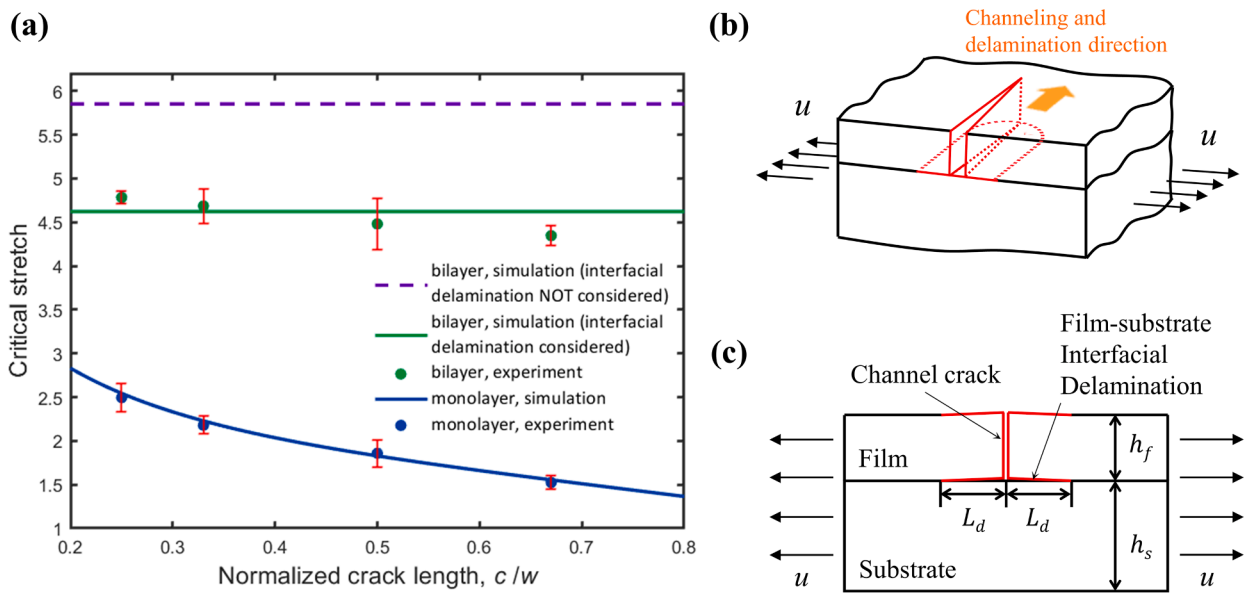

Fig. 8. Comparison between experimental results and theoretical predictions. (a) The numerically simulated and experimentally measured critical stretch to fracture plotted as a function of the normalized crack length c/w. For monolayer PAA hydrogel sheet, the experimentally measured critical stretches agree well with the numerical predictions. For bilayer PAAm-PAA structure, models with a well-bonded interface give predictions much higher than experimental measurements, while simulation results from models considering interfacial delamination (with normalized delamination width $L_d/h_f = 0.6$) match well with the experimental results. (b) Schematics illustrating steady-state co-evolving channel cracking and interfacial delamination. (c) Finite element models for calculating the energy release rate for co-evolving channel cracking and interfacial delamination. (For interpretation of the references to color in this figure, the reader is referred to the web version of this article.)

As evident in Inset II of Fig. 7d, the cross-sectional view of the crack shows that the crack with concomitant interfacial delamination opens widely in the wake of the crack front, with nearly uniform crack opening displacement through the film thickness, which is similar to the crack morphology in monolayer PAA sheets shown in Fig. 7b. The influence of the interfacial delamination on the fracture resistance of bilayer hydrogel structures will be investigated both experimentally and computationally in Sections 3.4 and 3.5.

3.4. Agreement between experimental measurements and theoretical predictions

We measure critical stretches of monolayer PAA films and PAAm-supported PAA films of various normalized crack lengths $c/w = 1/4, 1/3, 1/2, 2/3$. The dimensions of the PAA and PAAm samples being tested are 60 mm (gauge length between grips) × 10 mm (width) × 1.5 mm (thickness). Fig. 8a plots the experimentally measured critical stretches as a function of the normalized crack length c/w. At least 5 samples are tested to calculate the mean value and the standard derivation for each experimental data point. For the range of c/w investigated, the PAAm substrate can increase the critical stretches of monolayer PAA hydrogels by approximately a factor of two, further highlighting the effectiveness of the bilayer structural design in enhancing the fracture resistance of hydrogels.

Intriguingly, the critical stretch of PAAm-supported PAA sheets drops slightly as the normalized crack length c/w increases – this is not consistent with Eq. (6), which suggests the critical stretch for bilayer hydrogel structures is irrelevant to c/w. The discrepancy can be understood as follows: Eq. (6) is valid for steady-state crack propagation, which requires that the crack length c is sufficiently long compared to the film thickness h_f. Specifically, the crack length should exceed a few times the film thickness, and for more compliant substrates, the crack length to reach the steady state can be even longer (Ambrico and Begley, 2002; Huang et al., 2003; Nakamura and Kamath, 1992). Nevertheless, the c/h_f ratio of samples used in this study varies between 1.67 and 4.44, which does not fully meet the requirements for steady-state crack propagation. According to Ambrico and Begley (2002), before reaching steady-state propagation, the energy release rate for crack advancement rises with increasing c/h_f, thereby resulting in the slightly reduced critical stretches shown in Fig. 8a.

To compare experimental results shown in Fig. 8a to theoretical predictions, we next calculate critical stretches of monolayer PAA hydrogels and PAAm-supported PAA films based on the theoretical method presented in Section 2. According to Eqs. (10) and (6), to numerically predict the critical stretch of given monolayer and bilayer hydrogel structures – of which c, c/w, h_f, and h_s/h_f are given, one still needs to know the shear moduli of PAA and PAAm hydrogels as well as the fracture toughness of PAA hydrogels. Herein, we evaluate the shear moduli of PAA and PAAm hydrogels by fitting the incompressible neo-Hookean model to their uniaxial stress-stretch curves; the obtained shear modulus is 3kPa for PAA and 2.4kPa for PAAm, respectively (Appendix A). To obtain the fracture toughness, we substitute the experimentally measured critical stretch data of monolayer PAA hydrogel of $c/w = 0.5$ (i.e., $c = 5$mm) into Eq. (10) and the calculated fracture toughness for PAA hydrogel is $67.5 J/m^2$, which is consistent with our experimentally measured values (Appendix B) and those in the literature (Wang et al., 2019).

Once the fracture toughness of PAA and shear moduli of PAA and PAAm are known, critical stretches of monolayer PAA hydrogels and PAAm-supported PAA hydrogels can be readily determined by using Eq. (10) and Eq. (6), respectively. The results are included in Fig. 8a, where the theoretical predictions of the critical stretches of monolayer PAA hydrogels agree well with the experimental measurements – the differences between the experimental and computational results are within 2.25%. However, the computational predictions of the critical stretches of PAAm-supported PAA hydrogels are apparently higher than the experimental measurements, with discrepancies ranging from 22.4 to 34.6%. The difference can be attributed to the interfacial delamination observed in the bilayer structures, which will be discussed in detail in Section 3.5.

3.5. *Effect of interfacial delamination on the fracture resistance*

The co-evolution of film cracking and interfacial delamination has been common for substrate-film bilayer systems under large deformation (Li and Suo, 2007; Lu et al., 2007, 2009) since channel cracking and interfacial delamination facilitate each other. On the one hand, stress concentration on the interface near the channel root promotes interfacial delamination. On the other hand, as the film partially delaminates from the substrate, it induces a larger driving force for channel crack propagation. In this section, we quantitatively investigate the effect of interfacial delamination on the fracture resistance of substrate-supported hydrogel films.

Fig. 8b illustrates the co-evolution of channel crack and interfacial delamination in a bilayer structure subject to uniaxial tension. Under sufficiently large tension, the stress concentration near the channel root can be severe enough to induce interfacial delamination. During its propagation, the stresses can be analyzed based on the fracture process zone models, where the fracture process zone is assumed as a part of interfacial crack with ideal contact conditions ahead of the delamination front (Rose, 1987). According to Jia et al. (2011), under tension, the driving force for interfacial delamination decreases as the delamination advances in the tensile direction. As a result, when such a driving force becomes smaller than the interfacial toughness, the interfacial delamination eventually stops advancing in the tensile direction, ending up with a delamination width L_d in the undeformed configuration. On the other hand, the channel crack as well as the concomitant interfacial delamination of width L_d continues propagating in the direction perpendicular to the applied tension – a process defined as the steady-state co-evolution of channel crack and interfacial delamination.

To compute the total energy release rate G_{total} for the channel crack and the accompanying interfacial delamination of constant width L_d to advance in the direction normal to the applied tension, we use the same method employed in Section 2.2: We calculate the elastic energy stored in a slice of material of unit thickness far ahead of the crack front and that stored in a slice of material of unit thickness far behind the crack front (Fig. 8c), respectively. The elastic energy difference U between the two slices gives the energy release rate as $G_{total} = U/h_f$, where h_f denotes the film thickness.

Dimensional considerations indicate that the total driving force G_{total} takes a form similar to Eq. (2). That is,

$$G_{total} = q\left(\frac{L_d}{h_f}, \frac{h_s}{h_f}, \frac{\mu_s}{\mu_f}, \lambda_{appl}\right)\mu_f h_f. \tag{12}$$

In Eq. (12), the dimensionless function q depends on dimensionless parameters h_s/h_f, μ_s/μ_f, λ_{appl} and L_d/h_f, where the last dimensionless parameter L_d/h_f represents the normalized delamination width. The value of the dimensionless function q for any given bilayer structure can be evaluated after G_{total} is calculated by finite element simulations. The critical condition for steady-state co-evolving channel cracking and interfacial delamination is given by (Jia et al., 2011):

$$G_{total} = \Gamma_f + 2\Gamma_i L_d/h_f, \tag{13}$$

where Γ_f is the fracture toughness of the film as mentioned above and Γ_i is the interfacial toughness of the substrate-film interface. The second term on the right denotes the energy required for the interfacial delamination accompanying per unit area advance of the channel crack. By combining Eqs. (12) and (13), one can obtain the dimensionless form of the critical condition for the steady-state co-evolving channel cracking and interfacial delamination,

$$q\left(\frac{L_d}{h_f}, \frac{h_s}{h_f}, \frac{\mu_s}{\mu_f}, \lambda_{cr}^b\right) = \frac{\Gamma_f}{\mu_f h_f} + \frac{2\Gamma_i L_d}{\mu_f h_f^2}. \tag{14}$$

In the simulation, the incompressible Neo-Hookean model is adopted for both the substrate and the film, with the shear modulus experimentally measured to be 3kPa for the PAA film and 2.4kPa for the PAAm substrate (Appendix A). The thicknesses of the substrate and film are identical to those used in the experiments discussed in Sections 3.2 and 3.3. In addition, the fracture toughness Γ_f of the PAA hydrogel film has been evaluated as $67.5\text{J}/m^2$ in Section 3.4, and the interfacial toughness Γ_i of the PAAm-PAA interface is taken to be $40\text{J}/m^2$ according to the 180° peeling test (Appendix C) and the literature (Wang et al., 2019). To this end, once the normalized delamination width L_d/h_f is known, one can determine the critical stretch λ_{cr}^b for steady-state co-evolving channel cracking and interfacial delamination. As is conveyed by Fig. 8a, when setting the normalized delamination width $L_d/h_f = 0.6$, the predicted critical stretch – which is represented by the solid green line in the figure – matches the experimental results well, indicating that the

interfacial delamination is indeed the cause of the previously identified discrepancies between the experimental and simulation results mentioned in Section 3.4. Notably, although we cannot directly measure the delamination width L_d in the undeformed configuration in the experiment, the normalized delamination width $L_d/h_f = 0.6$ can be validated by the following fact: the experimentally measured crack opening displacement in the deformed configuration is consistent with the computationally simulated crack opening displacement when $L_d/h_f = 0.6$ (Appendix D).

It can be concluded from the above results that interfacial delamination of relatively small delamination width can result in an evident reduction in the critical stretch of the bilayer hydrogel structure. The phenomenon can be understood as follows: the interfacial delamination undermines the capability of the underlying substrate to constrain the crack opening displacement of the film, leading to higher energy release rate for channel cracking relative to bilayers with well-bonded interfaces, thereby causing reduced critical stretch. Therefore, designing bilayer hydrogel structures with mechanically strong film-substrate interfaces is critical for enhancing the fracture resistance of hydrogel film. Moreover, as illustrated in Fig. 8a, with the PAAm-PAA interface interlinked by noncovalent hydrogen bonds, the critical stretch of the bilayer PAAm-PAA structures is apparently higher than that of the monolayer PAA hydrogel, demonstrating the effectiveness of the fracture resistance enhancing strategy proposed in this work. To further improve the fracture resistance, one can strengthen the interface by using adhesion methods, including surface modification or topological adhesion, which depend on covalent bonds to enhance interfacial adhesion (Li et al., 2017a; Steck et al., 2020; Yang et al., 2020). Note here that the above analysis is based on the assumption that the underlying substrate has enough strength to withstand the severe stress concentration near the channel root. While in practical applications, this assumption is not necessarily tenable. Under such circumstances, the delamination may also have a positive effect on the whole structure's fracture resistance, on account of its relieving the stress concentration and thus protecting the substrate.

4. Conclusion

Considering the limitations of existing toughening methods towards improving the fracture toughness Γ of hydrogels, such as material-specific, complicated, or expensive synthesis processes, we have proposed a structure-based strategy to enhance the fracture resistance of hydrogels, which relies on constructing a film-substrate bilayer hydrogel system to reduce the energy release rate G for crack propagation. The advantages of the approach have been demonstrated through theoretical analysis, including (1) effectively enhancing the fracture resistance of hydrogels by several folds, and (2) rendering the fracture resistance of hydrogels independent of the crack length and the hydrogel size – which strongly affects the fracture resistance of monolayer hydrogels. To validate the theoretical prediction, we conduct experiments with PAA hydrogel films adhered to PAAm substrates. The experimental results show that a thin and compliant substrate can effectively enhance the critical stretch of PAA hydrogel films by reducing the crack opening displacement and energy release rate. Furthermore, it is experimentally observed that interfacial delamination may occur near the root of the channel crack. Theoretical predictions considering the interfacial delamination agree very well with the experimental results, validating the effectiveness of the structure-based fracture resistance enhancing strategy. The results from the present study, for the first time, offer a novel and unique "structural-toughening" approach for enhancing the fracture resistance of hydrogels by structurally regulating the energy release rate.

CRediT authorship contribution statement

Yijie Cai: Formal analysis, Methodology, Investigation, Software, Data curation, Writing – original draft. **Jie Ma:** Methodology, Formal analysis. **Zihang Shen:** Methodology, Formal analysis. **Xianmin Shao:** Formal analysis. **Zheng Jia:** Conceptualization, Methodology, Resources, Writing – review & editing, Supervision, Funding acquisition. **Shaoxing Qu:** Resources, Writing – review & editing, Supervision.

Declaration of Competing Interest

The authors declare that they have no known competing financial interests or personal relationships that could have appeared to influence the work reported in this paper.

The authors declare the following financial interests/personal relationships which may be considered as potential competing interests.

Data availability

No data was used for the research described in the article.

Acknowledgments

This work is supported by the National Natural Science Foundation of China (Grant Nos. 11802269 and 12072314), Natural Science Foundation of Zhejiang Province, China (Grant No. LR22A020005), and the 111 Project, China (Grant No. B21034).

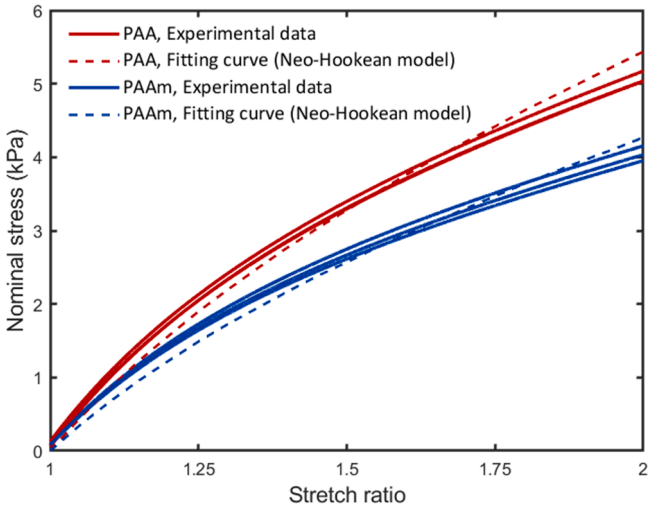

Fig. A1. Stress–stretch curves of PAA and PAAm hydrogels under uniaxial tension. Fitting the incompressible Neo-Hookean model (dashed curves) to the experimental stress–stretch curves (solid curves) gives the shear modulus of PAA and PAAm hydrogels.

Appendix A

To evaluate the shear modulus of PAA and PAAm hydrogels, we fit the incompressible neo-Hookean model to their uniaxial stress-stretch curves using the curve-fitting module of the commercial finite element code ABAQUS. It is indicated in Fig. A1 that proper fitting can be obtained at moderate stretches, yielding that shear modulus is 3kPa for PAA hydrogel and 2.4kPa for PAAm hydrogel used in the present work.

Appendix B

To validate the calculated fracture toughness for PAA hydrogel, we also conducted pure shear tests on PAA hydrogels. The dimensions of the PAA samples being tested are 70 mm (width W) $\times$ 17 mm (gauge height between grips H) $\times$ 1.5 mm (thickness), and

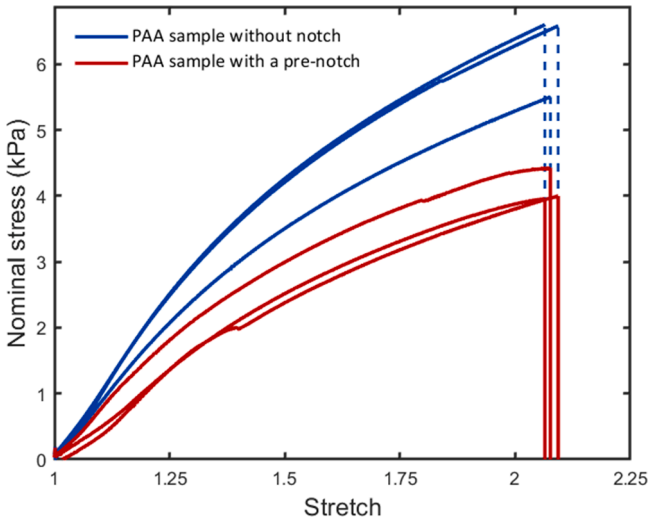

Fig. B1. The nominal stress-stretch curves of PAA hydrogels in pure-shear test for measuring the fracture toughness. The fracture toughness of the hydrogel is calculated as $\Gamma = H\int_1^{\lambda_c} s\mathrm{d}\lambda$, where H is the height of the PAA sample, λ_c is the critical stretch of the notched sample and s is the nominal stress of the sample without notch. (For interpretation of the references to color in this figure, the reader is referred to the web version of this article.)

the length of the pre-crack is $0.4W$. In the test, the notched PAA sample was stretched to a critical stretch of λ_c at which the crack propagates; the stress-stretch curves were recorded as the red lines in Fig. B1. Then, the unnotched hydrogel sheet was also stretched to λ_c with the stress-stretch curves recorded (the blue lines in Fig. B1). Based on the raw data in Fig. B1, the fracture toughness of the hydrogel can be calculated as $\Gamma = H\int_1^{\lambda_c} s d\lambda$, where H is the height of the PAA sample and s is the measured nominal stress. The experimentally measured fracture toughness of the three PAA samples is 61.6 J/m^2, 73.2 J/m^2 and 74.9 J/m^2, respectively, where the average is 69.9 J/m^2 and matches the fitting result (67.5 J/m^2) well.

Appendix C

The 180° peeling test is performed on the PAAm-PAA bilayer hydrogels to evaluate the interfacial toughness of the PAAm-PAA interface. The dimensions of the PAAm and PAA samples being tested are 70 mm (length L) × 20 mm (width W) × 1.5 mm (thickness T). Before testing, we glued inextensible polyester back layers on the top and bottom faces of the hydrogel samples using 406 Superglue (Loctite) to constrain the stretch of the peel arm. Then the ends of the back layers were clamped to the clamping fixtures of the testing machine. The sample was peeled by the machine at velocity $v = 30\ mm/min$, with the rate of peel set at $T/v = 3\ s$. During peel, the two arms were aligned vertically and the load cell recorded the peel force F. The ratios $2F/W$ of three identical samples are plotted as a function of the peel displacement in Fig. C1. The plateaus give the adhesion energy as 32.8 J/m^2, 40.6 J/m^2 and 45.2 J/m^2, respectively, where the specific value is determined by the built-in module of the test machine (SAS CMT-6103) and the average is 39.53 J/m^2.

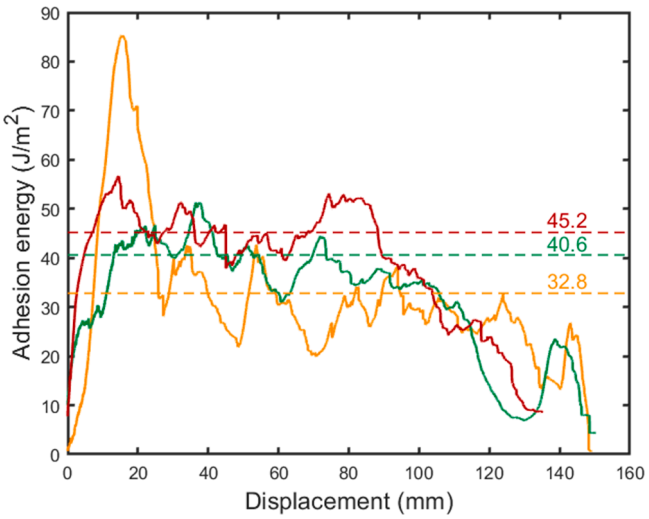

Fig. C1. Force-displacement curves of the adhered PAAm-PAA hydrogels in 180° peeling test for measuring the interfacial toughness. The adhesion energy is calculated as $2F/W$, where F is the peel force recorded by the load cell of the test machine and W is the width of the PAAm-PAA sample.

Appendix D

In Appendix D, we will validate that the normalized delamination width $L_d/h_f = 0.6$ – in the undeformed configuration – is reasonable. We focus on the largest crack opening displacement δ in the wake of the co-evolving channel crack and delamination (i.e., the distance between red dots in Fig. D1a). In the experiments, we record the deformation of PAAm-PAA bilayer hydrogels from the top view and acquire the critical crack opening displacement right before the propagation of channel cracking and interfacial delamination, which is $\delta_{cr} = 14.5$mm (Fig. D1b). In the simulations, the deformation of the bilayer structure in the wake of the channel crack can be accessible through modeling a slice of material of unit thickness far behind the crack front, according to the concept of steady-state crack propagation. While setting the normalized delamination width $L_d/h_f = 0.6$, we find the crack opening displacement under critical stretch is $\delta_{cr} = 15.2$mm (Fig. D1c), in good agreement with the experimentally measured value of 14.5mm. Hence, we verify that the normalized delamination width in the undeformed configuration $L_d/h_f = 0.6$ is reasonable.

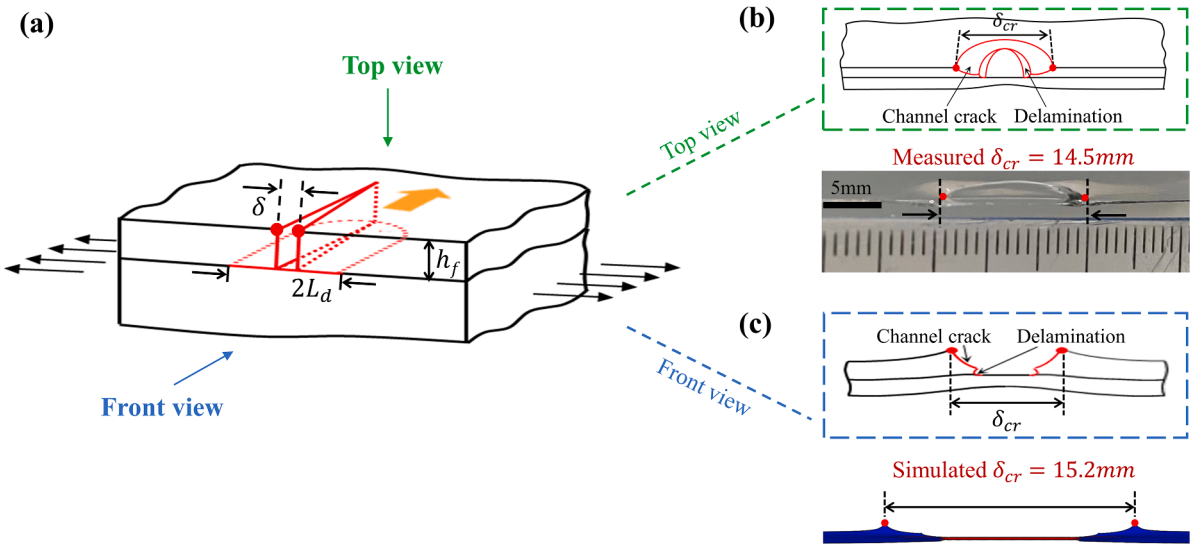

Fig. D1. Validation of the normalized delamination width $L_d/h_f = 0.6$. (a) Schematics of the co-evolving film cracking and interfacial delamination in film-substrate bilayer hydrogel structures. The largest crack opening displacement in the wake of the channel crack front δ – i.e., the distance between the two red dots in the schematics – is used for the validation. (b) Schematics and the experimental photo showing the deformation of PAAm-PAA hydrogel structures right before crack propagation. The crack opening displacement is measured to be $\delta_{cr} = 14.5$mm from the top view. (c) Schematics and the simulation result of the deformation of the bilayer hydrogel structure at critical stretch. With the normalized delamination width L_d/h_f setting to be 0.6, the simulated critical crack opening displacement $\delta_{cr} = 15.2$mm, which is consistent with the experimental measurements. (For interpretation of the references to color in this figure legend, the reader is referred to the web version of this article.)

References

Agrawal, A., Rahbar, N., Calvert, P.D., 2013. Strong fiber-reinforced hydrogel. Acta Biomater. 9, 5313–5318.
Ambrico, J.M., Begley, M.R., 2002. The role of initial flaw size, elastic compliance and plasticity in channel cracking of thin films. Thin Solid Films 419, 144–153.
Chen, Q., Zhu, L., Chen, H., Yan, H., Huang, L., Yang, J., Zheng, J., 2015. A novel design strategy for fully physically linked double network hydrogels with tough, fatigue resistant, and self-healing properties. Adv. Funct. Mater. 25, 1598–1607.
Cheng, J., Jia, Z., Guo, H., Nie, Z., Li, T., 2019. Delayed burst of a gel balloon. J. Mech. Phys. Solids 124, 143–158.
Cheng, J., Jia, Z., Li, T., 2020. A constitutive model of microfiber reinforced anisotropic hydrogels: with applications to wood-based hydrogels. J. Mech. Phys. Solids 138, 103893.
Cordero, N., Yoon, J., Suo, Z., 2007. Channel cracks in a hermetic coating consisting of organic and inorganic layers. Appl. Phys. Lett. 90, 111910.
Gong, J.P., Katsuyama, Y., Kurokawa, T., Osada, Y., 2003. Double-network hydrogels with extremely high mechanical strength. Adv. Mater. 15, 1155–1158.
Haghiashtiani, G., Habtour, E., Park, S.H., Gardea, F., McAlpine, M.C., 2018. 3D printed electrically-driven soft actuators. Extrem. Mech. Lett. 21, 1–8.
Hagiwara, Y., Putra, A., Kakugo, A., Furukawa, H., Gong, J.P., 2010. Ligament-like tough double-network hydrogel based on bacterial cellulose. Cellulose 17, 93–101.
Han, L., Lu, X., Wang, M., Gan, D., Deng, W., Wang, K., Fang, L., Liu, K., Chan, C.W., Tang, Y., Weng, L.T., Yuan, H., 2017. A mussel-inspired conductive, self-adhesive, and self-healable tough hydrogel as cell stimulators and implantable bioelectronics. Small 13, 1601916.
Haraguchi, K., Takehisa, T., 2002. Nanocomposite hydrogels: a unique organic–inorganic network structure with extraordinary mechanical, optical, and swelling/de-swelling properties. Adv. Mater. 14, 1120–1124.
Huang, R., Prévost, J.H., Huang, Z.Y., Suo, Z., 2003. Channel-cracking of thin films with the extended finite element method. Eng. Fract. Mech. 70, 2513–2526.
Hui, C.Y., Long, R., 2012. A constitutive model for the large deformation of a self-healing gel. Soft Matter 8, 8209–8216.
Hutchinson, J.W., Suo, Z., Hutchinson, J.W., Wu, T.Y., 1991. Mixed mode cracking in layered materials. Advances in Applied Mechanics. Elsevier, pp. 63–191.
Jang, J., Oh, H., Lee, J., Song, T.H., Jeong, Y.H., Cho, D.W., 2013. A cell-laden nanofiber/hydrogel composite structure with tough-soft mechanical property. Appl. Phys. Lett. 102, 211914.
Jia, Z., Tucker, M.B., Li, T., 2011. Failure mechanics of organic–inorganic multilayer permeation barriers in flexible electronics. Compos. Sci. Technol. 71, 365–372.
Keplinger, C., Sun, J.Y., Foo, C.C., Rothemund, P., Whitesides, G.M., Suo, Z., 2013. Stretchable, transparent, ionic conductors. Science 341, 984–987.
Kong, H.J., Wong, E., Mooney, D.J., 2003. Independent control of rigidity and toughness of polymeric hydrogels. Macromolecules 36, 4582–4588.

Lake, G.J., Thomas, A.G., 1967. The strength of highly elastic materials. Proc. R. Soc. Lond. A Math. Phys. Sci. 300, 108–119.
Larson, C., Peele, B., Li, S., Robinson, S., Totaro, M., Beccai, L., Mazzolai, B., Shepherd, R., 2016. Highly stretchable electroluminescent skin for optical signaling and tactile sensing. Science 351, 1071–1074.
Lee, Y., Song, W.J., Sun, J.Y., 2020. Hydrogel soft robotics. Mater. Today Phys. 15, 100258.
Li, J., Celiz, A.D., Yang, J., Yang, Q., Wamala, I., Whyte, W., Seo, B.R., Vasilyev, N.V., Vlassak, J.J., Suo, Z., Mooney, D.J., 2017a. Tough adhesives for diverse wet surfaces. Science 357, 378–381.
Li, T., Li, G., Liang, Y., Cheng, T., Dai, J., Yang, X., Liu, B., Zeng, Z., Huang, Z., Luo, Y., Xie, T., Yang, W., 2017b. Fast-moving soft electronic fish. Sci. Adv. 3, e1602045.
Li, T., Suo, Z., 2007. Ductility of thin metal films on polymer substrates modulated by interfacial adhesion. Int. J. Solids Struct. 44, 1696–1705.
Li, X., Yuan, L., Liu, R., He, H., Hao, J., Lu, Y., Wang, Y., Liang, G., Yuan, G., Guo, Z., 2021. Engineering textile electrode and bacterial cellulose nanofiber reinforced hydrogel electrolyte to enable high-performance flexible all-solid-state supercapacitors. Adv. Energy Mater. 11, 2003010.
Liao, I.C., Moutos, F.T., Estes, B.T., Zhao, X., Guilak, F., 2013. Composite three-dimensional woven scaffolds with interpenetrating network hydrogels to create functional synthetic articular cartilage. Adv. Funct. Mater. 23, 5833–5839.
Liu, X.J., Ren, X.Y., Guan, S., Li, H.Q., Song, Z.K., Gao, G.H., 2015. Highly stretchable and tough double network hydrogels via molecular stent. Eur. Polym. J. 73, 149–161.
Lu, N., Wang, X., Suo, Z., Vlassak, J., 2007. Metal films on polymer substrates stretched beyond 50%. Appl. Phys. Lett. 91, 221909.
Lu, N., Wang, X., Suo, Z., Vlassak, J., 2009. Failure by simultaneous grain growth, strain localization, and interface debonding in metal films on polymer substrates. J. Mater. Res. 24, 379–385.
Moutos, F.T., Freed, L.E., Guilak, F., 2007. A biomimetic three-dimensional woven composite scaffold for functional tissue engineering of cartilage. Nat. Mater. 6, 162–167.
Nakamura, T., Kamath, S.M., 1992. Three-dimensional effects in thin film fracture mechanics. Mech. Mater. 13, 67–77.
Nonoyama, T., Gong, J.P., 2015. Double-network hydrogel and its potential biomedical application: a review. Proc. Inst. Mech. Eng. Part H J. Eng. Med. 229, 853–863.
Qazi, T.H., Burdick, J.A., 2021. Granular hydrogels for endogenous tissue repair. Biomater. Biosyst. 1, 100008.
Rice, J.R., 1968. A path independent integral and the approximate analysis of strain concentration by notches and cracks. J. Appl. Mech. 35, 379–386.
Rose, L.R.F., 1987. Crack reinforcement by distributed springs. J. Mech. Phys. Solids 35, 383–405.
Sarwar, M.S., Dobashi, Y., Preston, C., Wyss, J.K.M., Mirabbasi, S., Madden, J.D.W., 2017. Bend, stretch, and touch: locating a finger on an actively deformed transparent sensor array. Sci. Adv. 3, e1602200.
Seitz, M.E., Martina, D., Baumberger, T., Krishnan, V.R., Hui, C.Y., Shull, K.R., 2009. Fracture and large strain behavior of self-assembled triblock copolymer gels. Soft Matter 5, 447–456.
Steck, J., Kim, J., Yang, J., Hassan, S., Suo, Z., 2020. Topological adhesion. I. Rapid and strong topohesives. Extrem. Mech. Lett. 39, 100803.
Sun, J.Y., Zhao, X., Illeperuma, W.R.K., Chaudhuri, O., Oh, K.H., Mooney, D.J., Vlassak, J.J., Suo, Z., 2012. Highly stretchable and tough hydrogels. Nature 489, 133–136.
Wang, Q., Gao, Z., 2016. A constitutive model of nanocomposite hydrogels with nanoparticle crosslinkers. J. Mech. Phys. Solids 94, 127–147.
Wang, Q., Mynar, J.L., Yoshida, M., Lee, E., Lee, M., Okuro, K., Kinbara, K., Aida, T., 2010. High-water-content mouldable hydrogels by mixing clay and a dendritic molecular binder. Nature 463, 339–343.
Wang, Y., Jia, K., Xiang, C., Yang, J., Yao, X., Suo, Z., 2019. Instant, tough, noncovalent adhesion. ACS Appl. Mater. Interfaces 11, 40749–40757.
Wang, Y., Liang, D., Suo, Z., Jia, K., 2020. Synergy of noncovalent interlink and covalent toughener for tough hydrogel adhesion. Extrem. Mech. Lett. 39, 100797.
Wathoni, N., Motoyama, K., Higashi, T., Okajima, M., Kaneko, T., Arima, H., 2016. Physically crosslinked-sacran hydrogel films for wound dressing application. Int. J. Biol. Macromol. 89, 465–470.
Yang, C., Yin, T., Suo, Z., 2019. Polyacrylamide hydrogels. I. Network imperfection. J. Mech. Phys. Solids 131, 43–55.
Yang, J., Steck, J., Bai, R., Suo, Z., 2020. Topological adhesion II. Stretchable adhesion. Extrem. Mech. Lett. 40, 100891.
Yao, X., Chen, B., Morelle, X.P., Suo, Z., 2021. Anti-icing propylene-glycol materials. Extrem. Mech. Lett. 44, 101225.
Yiming, B., Liu, T., Nian, G., Han, Z., Jia, Z., Qu, S., 2020. Mechanics-guided design of shape-morphing composite sheets with hard and soft materials. Extrem. Mech. Lett. 35, 100643.
Yin, H., King, D.R., Sun, T.L., Saruwatari, Y., Nakajima, T., Kurokawa, T., Gong, J.P., 2020. Polyzwitterions as a versatile building block of tough hydrogels: from polyelectrolyte complex gels to double-network gels. ACS Appl. Mater. Interfaces 12, 50068–50076.
Zhao, X., 2012. A theory for large deformation and damage of interpenetrating polymer networks. J. Mech. Phys. Solids 60, 319–332.
Zhao, X., Huebsch, N., Mooney, D.J., Suo, Z., 2010. Stress-relaxation behavior in gels with ionic and covalent crosslinks. J. Appl. Phys. 107, 063509.